HIGH PERFORMANCE HEAT EXCHANGER WITH OBLIQUE-WAVE WALLS

Y. Suzue, K. Morimoto, N. Shikazono, Y. Suzuki and N. Kasagi
Department of Mechanical Engineering, The University of Tokyo,
Hongo 7-3-1, Bunkyo-ku, Tokyo 113-8656, JAPAN

Abstract

A series of numerical simulation of the convective heat transfer in a duct with obliquely wavy surfaces is carried out in order to develop high performance heat exchangers. The effects of geometrical parameters are examined to optimize the heat exchanger duct design. The heat transfer rate of the oblique-wave duct is correlated fairly well and increases with the Reynolds number based on the wave amplitude and the bulk mean velocity, while the resultant j/f factor becomes saturated due to marked increase in the pressure drag. When the duct aspect ratio is increased, the j/f factor is also increased, although the heat transfer coefficient itself is suppressed because the surface-induced secondary flow weakens. By arranging the adjacent waves in opposing oblique angles in the case of a parallel plate channel, intense secondary flow is generated. This makes the heat transfer coefficient significantly improved, whilst the j/f enhancement remains relatively small due to the large pressure drop. It is found that, at the optimal point, the proposed oblique-wave heat exchanger achieves a 16% volume reduction from the existing cross corrugated heat exchangers.

Nomenclature

D_h	Hydraulic Diameter	δ	Half duct height
f	Fanning friction factor, equation (3)	γ	Oblique angle, see Figure 1
j	Colburn j factor, equation (7)	ΔT_{lm}	Log-mean temperature difference, equation (8)
S_{total}	Total heat transfer surface area		
$T_{w,m}$	Wall mean Temperature	τ_w	Streamwise wall shear stress
y_w	Deformation of wavy walls, equation (1) and (2)		

1. Introduction

Because of the growing demands for saving energy and mitigating environmental impacts, high performance heat exchangers have become ever more important in various equipment such as automobiles and distributed energy systems. Uechi *et al.* (2004) proposed a micro gas turbine and fuel cell hybrid system of 30-kW power output with generation efficiency over 65%, and they showed that the recuperator effectiveness should be one of the most important technical issues to improve the system efficiency.

Among various types of compact heat exchangers, the primary surface recuperator (PSR) has been considered as the most promising candidate for gas turbine usage, because of its design simplicity and high thermal effectiveness (McDonald, 2000). Recently, Morimoto *et al.* (2005) demonstrated that the employment of obliquely wavy heat transfer surfaces in a square duct can offer significant heat transfer enhancement with relatively small pressure loss penalty. This concept is presently examined in more general cases of rectangular ducts or plain channels for various heat exchanger applications.
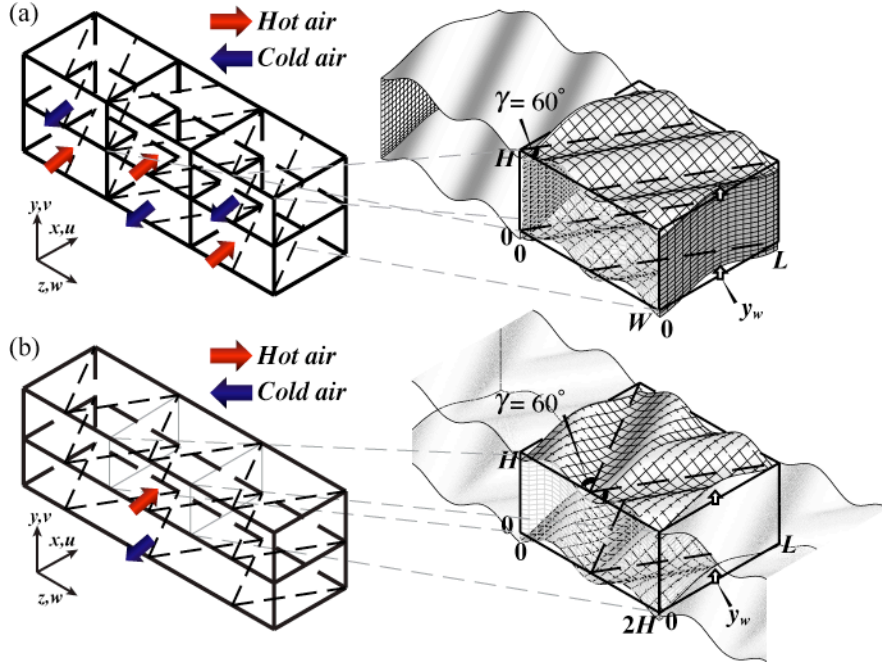
Figure 1. Schematic view and computational domain of oblique-wave heat exchangers:
(a) rectangular duct (Case I), (b) parallel plate channel (Case II).

The main objectives of the present study are to apply the obliquely wavy surface concept to rectangular ducts with different aspect ratios and also to parallel plate channels, and to obtain general guidelines for the better compact heat exchanger design. Therefore, the heat transfer and pressure loss characteristics of oblique-wave heat exchangers with different geometrical parameters are examined in detail through a series of numerical simulation.

2. Heat Exchanger Configuration

Two types of counter-flow heat exchangers are examined in this study, *i.e.*, rectangular duct (Case I) and parallel plate channel (Case II). Figure 1 shows the present heat exchanger configuration and the surface topology over one pitch with computational grids. Note that, in Case II, adjacent waves are directed in two symmetrical oblique directions.

2.1 Rectangular Duct (Case I)

The top and bottom walls of straight rectangular ducts with the height H and the width W are replaced by the same obliquely wavy surfaces, whilst the left and right walls are kept flat. The wall deformation of top and bottom surfaces (y_w) is defined as:

$$y_w = -A\cos\frac{2\pi}{L}\left\{x-(W/H)z\tan\gamma\right\},\tag{1}$$

where A, L, and γ denote the amplitude, spanwise pitch and oblique angle of the waves, respectively. Each passage is surrounded by oblique-wave walls and flat side walls, and hot and cold fluids flow in a staggered counterflow arrangement. The thermal resistance of dividing walls is generally much smaller than the convective one, and neglected throughout this study. The oblique angles are equal in magnitude but opposite in sign for the adjacent passages.

2.2 Parallel Plate Channel (Case II)

In Case II, the top and bottom walls of parallel plate channels are corrugated into W-shaped surfaces by combining oblique-waves defined by equation (1). Then, the surface geometry is given as follows:

$$y_w = \begin{cases} -A\cos\dfrac{2\pi}{L}(x - z\tan\gamma) & (2m \le z/H \le 2m+1) \\[2mm] -A\cos\dfrac{2\pi}{L}(x + z\tan\gamma) & (2m+1 \le z/H \le 2m+2) \end{cases}, \tag{2}$$

where m denotes any integer. Thus, the oblique angle changes its sign along the z-direction at $z/H = m$.

3. Numerical Procedure

The governing equations are the incompressible Navier-Stokes, continuity, and energy equations. The present numerical scheme is based on the finite difference method with general coordinate system. The flow is advanced in time by employing a second-order Adams-Bashforth scheme and a Crank-Nicolson scheme for the nonlinear and the viscous terms, respectively. Continuity is ensured with the SMAC method. Both of the counter-flowing fluids are air (Prandtl number, Pr = 0.71), and the bulk mean temperature is kept constant at each inlet. In order to obtain fully-developed flow and thermal fields, a periodic boundary condition (Patankar $et\ al.$, 1977) is imposed in the streamwise direction in Cases I and II, and also in the spanwise direction in Case II. No-slip boundary condition is imposed on the wall surfaces, and the thermal coupling with the neighboring passages is considered by assuming the temperature and the heat flux to be continuous at the dividing walls.
In this study, the Reynolds number Re_{Dh}, based on the bulk mean velocity U_b and hydraulic diameter D_h ($= 4V/S_{total}$), is varied from 100 to 1000, considering the suitable range for gas turbine usage.

The Fanning friction factor and the averaged wall shear stress are defined as follows:

$$f = \frac{(\Delta p / L) D_h}{2\rho U_b^{\ 2}}, \tag{3}$$

$$\langle \tau_w \rangle = \frac{1}{S_{total}} \frac{2D_h}{U_b} \int_S \frac{\partial u}{\partial n'} dS, \tag{4}$$

where Δp represents the mean pressure difference between the inlet and outlet of the passage, and n' refers to y coordinate for the top and bottom walls and z for the left and right walls. The heat transfer coefficient h, the average Nusselt number Nu, and the Colburn j factor are defined as follows:

$$h = \frac{q}{\Delta T_{lm}} = \frac{1}{S_{total}\Delta T_{lm}} \int_S \left(-k\frac{\partial T}{\partial n} \right) dS, \tag{5}$$

$$\mathrm{Nu} = \frac{hD_h}{k}, \tag{6}$$

$$j = \frac{\mathrm{Nu}\,\mathrm{Pr}^{-1/3}}{\mathrm{Re}_{D_h}}, \tag{7}$$

where the logarithmic mean temperature difference ΔT_{lm} is defined by

$$\Delta T_{lm} = \frac{T_b(L) - T_b(0)}{\ln\{T_{w,m}(0) - T_b(0)\} - \ln\{T_{w,m}(L) - T_b(L)\}} . \qquad (8)$$

The number of grid points is $32 \times 37 \times (36 \cdot (W/H) + 1)$ in the x-, y- and z-directions, respectively. A uniform mesh is used in the x-direction, while nonuniform meshes of hyperbolic tangent distribution are used in the y- and z-directions for the grid points to become dense near the wall and the symmetry plane. The grid spacing in each direction is given as Table 1. In straight square duct, the difference of the computed values and the analytical solution (Shah and London, 1978) is less than 0.3% both for the friction factor and the Nusselt number, and the second-order accuracy of the spatial discretization is confirmed by doubling the number of grids in each direction. We have also examined the effect of the grid spacing on the calculated results in some cases of wavy duct, and have confirmed the grid independency of the present computational results. The time increment Δt, nondimesionalized by U_b and half duct height δ, is 0.01. The initial flow field is given as the analytical solution in a straight rectangular duct or a parallel channel. Most simulation cases require about 4000 time steps ($t = 40$) to reach a steady state, where the convergence criteria of the residual of the continuity equation being less than 10^{-6} is satisfied. All results shown in this paper are laminar steady-state solutions obtained by the aforementioned time-marching calculation.

4. Results and Discussion

Throughout the present study, the oblique angle γ is kept to be 60 degrees, with which the maximum j/f factor is obtained in the case of duct aspect ratio $W/H = 1$ (Morimoto *et al.*, 2005).

4.1 Results for Case I: Rectangular Ducts

First, the duct aspect ratio W/H is set to unity, and the effects of wave amplitude are examined at $A/H = 0.05$, 0.10 and 0.15. Here, we introduce another Reynolds number Re_A based on the wave amplitude A and the bulk mean velocity U_b.

Figure 2 shows the heat transfer coefficient h and the j/f factor, both of which are normalized by those of a straight rectangular duct of the same height and width, against Re_A for different wave amplitudes. Both factors are significantly enhanced in a wide range of Re_A. It is also seen that the heat transfer coefficient of h is correlated well with Re_A regardless of the amplitude (see, Figure 2(a)), whereas the j/f factor is also dependent on the wave amplitude. The different enhancement rate in j/f becomes evident at higher Re_A, and this fact is owing to the marked increase of pressure loss. It is clear from Figure 2(a) that the wave amplitude should be chosen to get a sufficiently large value of Re_A to meet required heat transfer enhancement under prescribed flow conditions.

The effect of aspect ratio is examined at $W/H = 1$, 2, 4 and 8 with the wave amplitude kept constant

Table 1. Grid resolution of the present simulation.

Number of grid points	Grid spacing				
N_x, N_y, N_z	$\Delta x / \delta$	$\Delta y_{min} / H$	$\Delta y_{max} / H$	$\Delta z_{min} / H$	$\Delta z_{max} / H$
32, 37, 37 ~ 289	1.08×10^{-2}	4.65×10^{-2}	6.10×10^{-2}	$4.58 \times 10^{-2} \sim 4.64 \times 10^{-2}$	6.10×10^{-2}
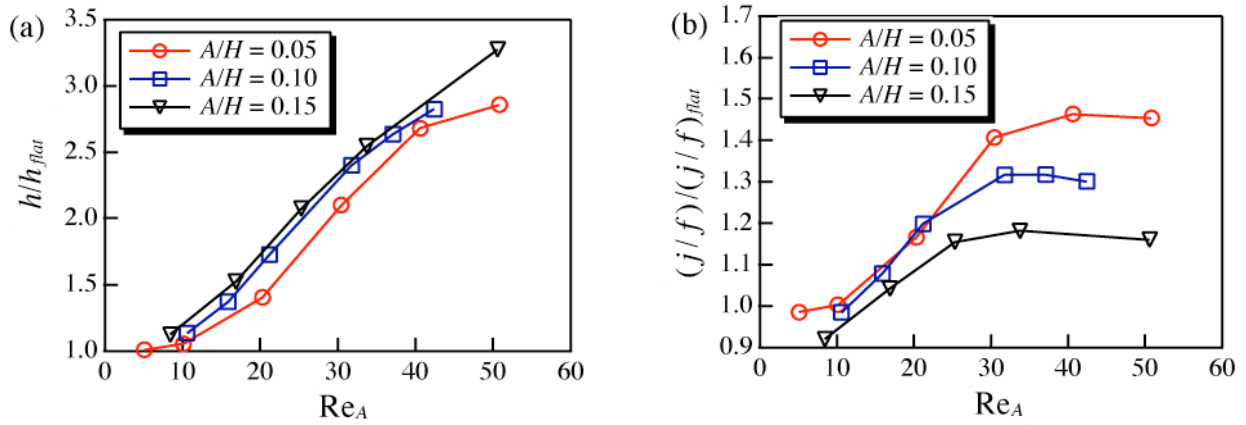
Figure 2. Effects of wave amplitude and Re_A; (a) Averaged heat transfer coefficient, (b) j/f factor.
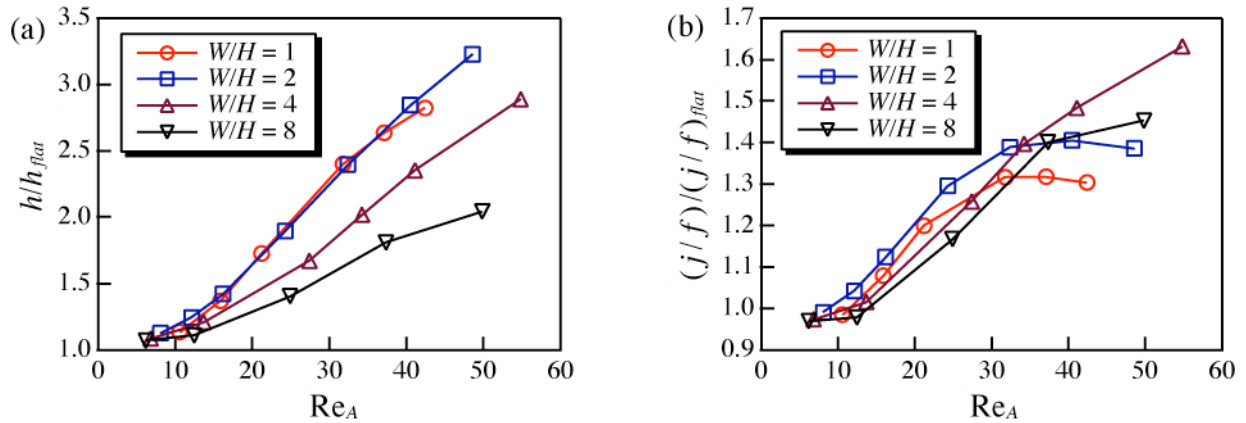
Figure 3. Effects of flow passage aspect ratio and Re_A; (a) Averaged heat transfer coefficient, (b) j/f factor.

($A/H = 0.1$). The spanwise wavelength of the wavy surfaces is set to be H, so that the spanwise wave number is equal to the duct aspect ratio. Figure 3 shows the heat transfer coefficient h and the j/f factor versus Re_A for different aspect ratios. Both quantities are markedly enhanced when Re_A is larger than 10, regardless of the duct aspect ratio. In contrast to Figure 2, the enhancement ratio of h decreases as the aspect ratio increases, while the j/f factor becomes extremely large at higher Re_A. It is noted that the pressure drop is much increased with Re_A due to the flow separation, when the aspect ratio is small (see, Figure 3(b)).

Figure 4 shows the wall shear stress vectors on the bottom wall and iso-coutours of the streamwise wall shear stress at $W/H = 2$, $Re_A \sim 16$, and $Re_{Dh} = 200$. It is shown that a high shear stress region is generated along the hill from the left wall, and that flow separation occurs at the one edge of wave valleys ($z/H = 0$, denoted as **A**).

Figure 5 shows the velocity vectors and temperature contours in the y-z plane at $W/H = 2$, $Re_A \sim 16$, and $Re_{Dh} = 200$. Vortical structures can be observed around the crest of wavy walls. Almost the same heat transfer performance is obtained on the left and right walls, because high- and low-speed flows appear on each side of the dividing wall in this counter-flow arrangement. In addition, the velocity and temperature distributions of hot and cold fluids become symmetrical across the top and bottom walls, so that the heat transfer enhancement is achieved over wide areas. Especially, the enhancement of j/f factor is remarkable on the top and bottom walls, where the intense secondary flow is induced (circled region in Figure 5).

As the duct aspect ratio increases, the magnitude of the secondary flow decreases ($0.28U_b$ and $0.24U_b$ for $W/H = 1$ and 2, respectively), while the total heat transfer surface area increases. Thus
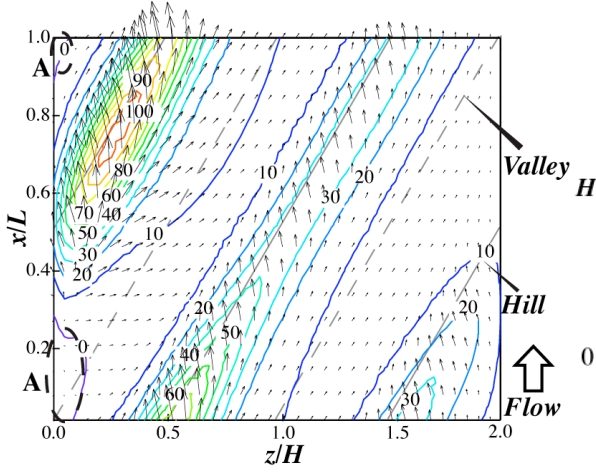
Figure 4. Shear stress vectors and contours of streamwise shear stress on the bottom wall ($Re_A \sim 32$, $W/H = 2$).
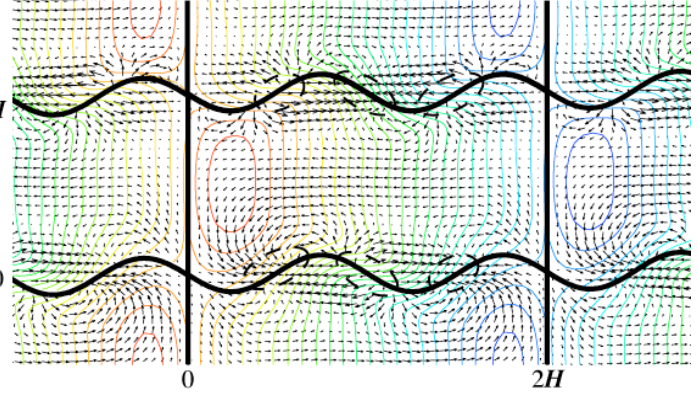
Figure 5. Velocity vectors and temperature contours in y-z plane at $x/L = 0.25$: $A/H = 0.1$, $W/H = 2$. Contour increment is $0.1(T_{H,in} - T_{C,in})$
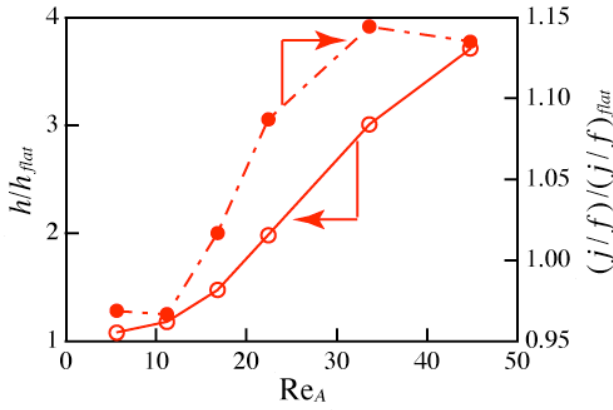
Figure 6. Averaged heat transfer coefficient h and j/f factor for Case II.
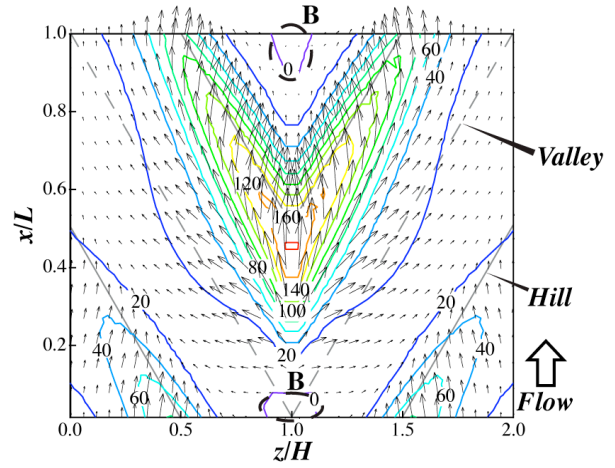
Figure 7. Shear stress vectors and contours of streamwise shear stress on the bottom wall (Case II, $Re_A \sim 32$).

the maximum heat transfer coefficient is obtained at $W/H = 2$. In terms of h and j/f, the benefit of oblique-wave walls is most significant at $W/H = 2$.

4.2 Results for Case II: Parallel Plate Channel

In this section, performance of the parallel plate channel with W-shaped wavy walls is examined. As shown in the previous section, a wider aspect ratio does not simply offer substantial heat transfer enhancement. Thus, in parallel plate channels, of which W/H is infinity, we employ the W-shaped wave corrugation described by equation (2). It is expected that W-shaped wave corrugation may give similar flow pattern as the low-aspect-ratio duct flow, because of its symmetrical configuration.

Figure 6 shows the augmentation ratio of the heat transfer coefficient h and the j/f factor for different Re_A. The increase of h is larger in Case II than in Case I. Although the enhancement ratio of j/f factors is relatively small, it is still higher than that of flat parallel plate channels at high Re_A. Therefore, the oblique-wave concept is also effective for the parallel plate channels.

Figure 7 shows the wall shear stress vectors on the bottom walls with iso-contours of the streamwise wall shear stress. It is seen that high shear stresses are induced along the hill, and that the magnitude is more intense than in Case I.
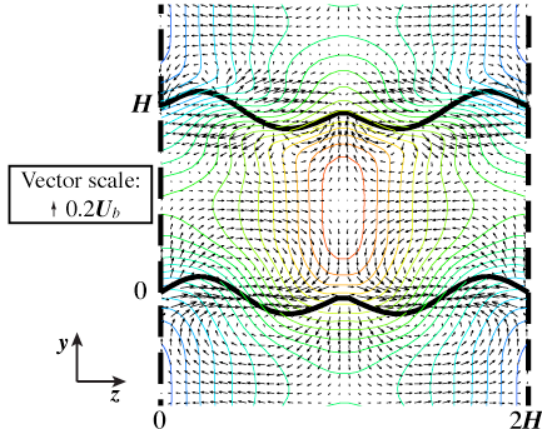
Figure 8. Velocity vectors and temperature contours for Case II in *y-z* plane at *x/L* = 0.25: Contour increment is $0.1(T_{H,in} - T_{C,in})$
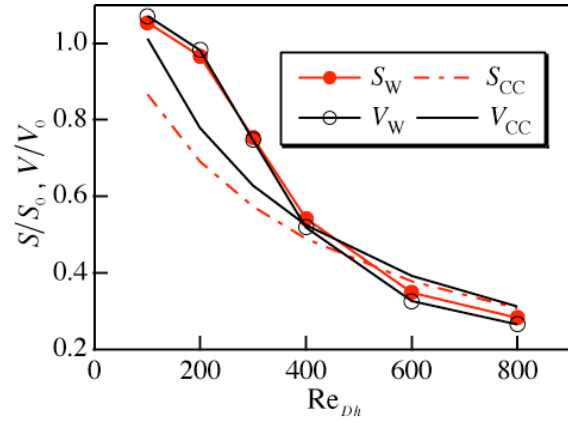
Figure 9. Area and volume comparison between obliquely wavy and existing CC surface.

Figure 8 shows the velocity vectors and temperature contours in the *y-z* plane at $Re_A \sim 16$ and Re_{Dh} = 300. It is clearly observed that the W-shaped wavy surface induces counter-rotating vortices even without the side walls. Temperature contours are distorted toward the W-edge of the wall (*z/H* = 1). The maximum magnitude of this secondary flow is about $0.32U_b$, which is larger than that in Case I. Both pressure and friction drags are significantly increased with increasing Re_A. In particular, the pressure drag is significantly increased by the flow separation at the valley of the W-edge pointing upstream (denoted as **B** in Figure 7).

4.3 Heat Exchanger Performance Evaluation

From the above results, the effectiveness of obliquely-wavy surface heat exchangers is evaluated. Two kinds of heat transfer performance indices for compact heat exchangers are examined; *i.e.*, the total volume ($f\,Re/\,j^2$) and the total heat transfer surface area ($f\,Re^{1/2}/\,j^{3/2}$) for a constant pumping power and NTU (Cowell, 1990). In Figure 9, the normalized volume and surface area of the parallel plate channel with W-shaped corrugation (denoted with the subscript W) are compared with those of the existing high performance heat transfer surface (cross corrugated surface; Utriainen and Sundén, 2002) (denoted as CC). When the Reynolds number Re_{Dh} is small, the CC surface is better in terms of both indices because of its high heat transfer performance.

However, when Re_{Dh} is larger than 400, significant heat transfer enhancement is achieved by the W-wave parallel plate, so more compact heat exchanger design becomes possible. Because of the larger *j/f* factor, both frontal area and volume reductions are achieved. At the optimal point (Re_{Dh} = 800), the volume reduction rate from the flat channels exceeds the CC surface by 5%, and a 16% volume reduction from the CC surfaces is achieved.

5. Conclusions

Fully-developed velocity and temperature fields in the oblique-wave heat exchangers of different geometrical parameters have been numerically simulated in order to examine their performances.

The maximum enhancement of the heat transfer coefficient *h* and the *j/f* factor is achieved at *W/H* ~ 2 in the case of rectangular duct. At larger aspect ratios, the augmentation ratio of *j/f* is sustained, but the enhancement of *h* is saturated due to the weakened secondary flows. The heat transfer coefficient is correlated fairly well with the wave amplitude Reynolds number Re_A, which is identified as an important parameter for the oblique-wave heat exchangers. However, the effect of

pressure drag is increased at large wave amplitudes. Therefore, under a given velocity condition, the wave amplitude should be chosen to avoid excessive increase of pressure drag.

Contrary to the rectangular ducts, significant heat transfer enhancement is achieved in the parallel plate channel by employing the W-shaped wave corrugation. This is due to the intense secondary flow induced by the W-shaped waves. The parallel plate channels with W-shaped wave corrugation can offer an advantage of reducing the volume and surface area more than the conventional cross-corrugated surface when Re_A is large.

References

Cowell, T. A., 1990, A general method for the comparison of compact heat exchanger surfaces, ASME J. Heat Transfer, 112, 288-294.

McDonald, C.F., 2000, Low-cost compact primary surface recuperator concept for microturbines, Appl. Therm. Eng., 20, 471-497.

Morimoto, K., Suzuki, Y. and Kasagi, N., 2005, Optimal Shape Design of Counter-Flow Primary Surface Recuperators, Proc. 5th Int. Conf. Enhanced, Compact and Ultra-Compact Heat Exchangers, Paper CHE2005-17, 124-131.

Patankar, S. V., Liu, C. H. and Sparrow, E. M., 1977, Fully Developed Flow and Heat Transfer in Ducts Having Streamwise-Periodic Variations of Cross-Sectional Area, ASME J. Heat Transfer, 99, 180-186.

Shah, R. K. and London, A. L., 1978, Laminar Flow Forced Convection in Ducts, Advances in Heat Transfer, Supplement 1, Academic Press, New York.

Uechi, H., Kimijima, S. and Kasagi, N., 2004, Cycle Analysis of Gas Turbine-Fuel Cell Hybrid Micro Generation System, ASME J. Eng. Gas Turbines Power, 126, 755-762.

Utriainen, E. and Sundén, B., 2002, Evaluation of the Cross Corrugated and Some Other Candidate Heat Transfer Surfaces for Microturbine Recuperators, ASME J. Eng. Gas Turbines Power, 124, 550-560.